Bond Graph Based Stability Analysis of a Railway Traction System

Grace Gandanegara, Xavier Roboam, Bruno Sareni, Geneviã¨ve Dauphin-Tanguy

Bond Graph Based Stability Analysis of a Railway Traction System

G. Gandanegara[1], X. Roboam[1], B. Sareni[1], G. Dauphin-Tanguy[2]

[1] *LEEI, UMR INPT-ENSEEIHT/CNRS No. 5828 - 2 rue Camichel - BP 7122 - 31071 Toulouse Cedex 7 – France*
e-mail : Xavier.Roboam@leei.enseeiht.fr

[2] *LAGIS, Ecole Centrale de Lille, UMR CNRS No. 8146 - BP 48 - 59651 Villeneuve d'Ascq Cedex – France*
e-mail : gdt@ec-lille.fr

Abstract
This paper emphasises the interest of the Bond Graph approach for analysis and system design of heterogeneous and multi-field devices. In particular, the local stability analysis of non linear systems can be directly derived from the linearised Causal Bond Graph. This method is applied to a typical electrical engineering system : a railway traction device involving electromechanical couplings. Validity, usefulness and originality of this approach are displayed.

Keywords : *Bond graph, system design, heterogeneous devices, modelling, stability.*

I. INTRODUCTION

Electrical engineering systems are more and more complex and heterogeneous, being constituted by elements of different natures and different physical fields. In order to face these issues, a unified formalism is particularly useful : the Bond Graph (BG) [1-3] has been conceived in this way to represent power transfers by establishing energetic analogies between each field. The causality, essential property for power systems, is graphically represented in the BGs. Several interesting properties can be directly derived from the Causal Bond Graph in terms of system analysis and design:

- Homogeneous modelling of a heterogeneous system makes easier coupling analysis by means of causal properties;
- Several analysis methods are directly applicable on BGs, such as structural or modal analysis [3-5], stability analysis, model simplification methods [6-12];
- An inverse modelling of the system can be obtained by means of bi-causality concept [13] allowing to synthesize constraints relative to system requirements at each level of the BG.

In this paper, a railway traction system is considered as case study. A bond graph model of this typical non linear system in electrical engineering allows to analyse the stability. For this purpose, the system is linearised thanks to the linearised BG [14]. This paper is divided in four sections:

- Firstly, a short review of the BG formalism is described.
- Several analysis techniques, directly applicable on BGs are presented in section III, in particular for the stability analysis.
- The modelling of the railway traction device is presented in the fourth section : an original BG of AC induction motors is described especially when the system must be linearised around an operating point in order to achieve the stability analysis.
- The fifth section shows the stability analysis of the obtained models.

II. BOND GRAPH BASIC PRINCIPLES

The BG formalism [1-3], introduced by H. Paynter in 1961 and formalised by Karnopp and Rosenberg in 1975, is now regularly used in many companies, particularly in automobile industry (PSA, Renault, Ford, Toyota, General Motors, …). This graphical method illustrates the energetic transfers in the system. The orientation of a half arrow indicates the power flow as expressed in Fig. 1. The primary characteristic of the BG is relative to its unified aspect through analogies summarised in Table 1. It obviously shows that this method can be applied to all physical domains by using generalised variables for :

- power : effort e (voltage in electricity) and flow f (current in electricity),
- energy : moment p (integral of effort) and displacement q (integral of flow).

Table 1. Generalised variables in several domains.

Field	**Effort *e***	**Flow *f***	**Moment *p***	**Displacement *q***
Electrical	Voltage u	Current i	Magnetic flux Φ	Charge q
Mechanical Translation	Force F	Speed v	Impulse p	Displacement x
Mechanical Rotation	Torque T	Angular Speed ω	Angular impulse h	Angle θ
Hydraulic	Pressure P	Flow Q	Pressure impulse Γ	Volume V
Chemical	Chemical potential	Molar flow	-	Number of moles
Thermodynamic	Temperature T	Entropy flow	-	Entropy

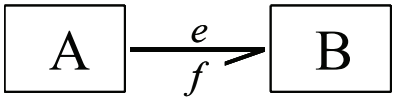

Fig. 1. Bond graph power transfer.

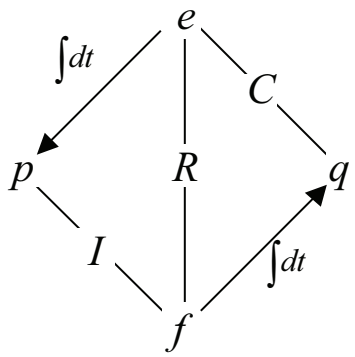

Fig. 2. Paynter's tetrahedron.

Each bond brings simultaneously both information of effort and flow, where the product gives the transmitted power. Elements can be connected with 0-junctions (common effort), 1-junctions (common flow), transformers *TF* (relations effort-effort and flow-flow) and gyrators *GY* (relations effort-flow). These junctions are considered as power conservative. Active elements for effort and flow sources are added with three types of passive elements, each one representing storage or dissipative interactions between generalised variables as displayed by Paynter's tetrahedron in Fig. 2.

One of the most important bond graph properties for system analysis and design is the causality. It is graphically described by the "causal stroke" :

A imposes its effort to B whose the consequence is its flow

B imposes its effort to A whose the consequence is its flow

Fig. 3. Causality assignments.

Properties of causal BGs are particularly rich in information :

- As power transfers are concerned, they indicate if basic physical rules have been fulfilled when several elements are coupled. Indeed, respecting the integral causality ensures that the association is physically (and energetically) convenient and then "numerically consistent";
- By following the causal loops and causal paths in the BGs, one can analyse couplings between elements in spite of domain changes;
- Many properties, useful for system analysis, can be extracted (see section III).

Simplified example :

Better than detailing the Bond Graph theory, which has been developed in several references [1-3], we illustrate this approach with the simple example of a DC traction system (see Fig. 4). The DC-DC converter is supposed to be perfect and power conservative. It can then be modelled as a modulated transformer (*MTF*). If an instantaneous model is considered the modulation of the transformer is relative to the firing order state of the chopper (C_H). In average values, the gain is relative to the duty cycle following (eq. 1) :

$$\begin{aligned} V_m &= \alpha V_{Cf} \\ I_H &= \alpha I_m \end{aligned} \qquad \text{(eq. 1)}$$

where I_H and V_{Cf} denote the output current and voltage of the LCR filter, V_m and I_m represent the input current and voltage of the DC motor.

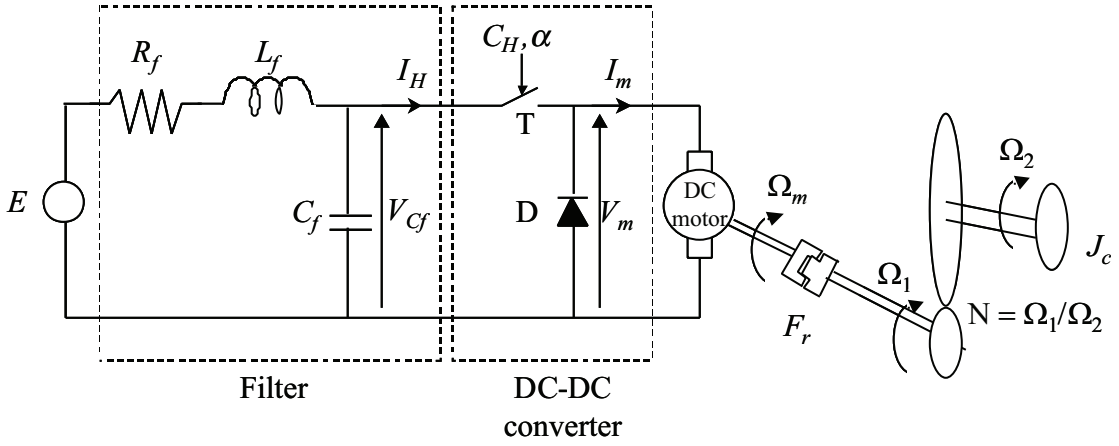

Fig. 4. DC motor traction system.

The electromechanical coupling represented by (eq. 2) can be modelled by a gyrator (*GY*) crossing electrical effort (i.e. the emf E_m) with the mechanical flow (the rotation speed Ω_m) and the mechanical effort (i.e. the em torque T_{em}) with the flow (i.e. the current I_m) on the electrical side.

$$\begin{aligned} E_m &= K\,\Omega_m \\ T_{em} &= K\,I_m \end{aligned} \qquad \text{(eq. 2)}$$

The motor is coupled with a mechanical load through a reducer. The associated causal BG with integral (physical) causality is represented by Fig. 5. For example, the causal analysis of the input filter shows that the inductance L_f imposes a common current (junction 1) in the E, R_f, L_f branch, while the capacitor (C_f) imposes its effort (voltage) to other elements placed in parallel (junction 0).

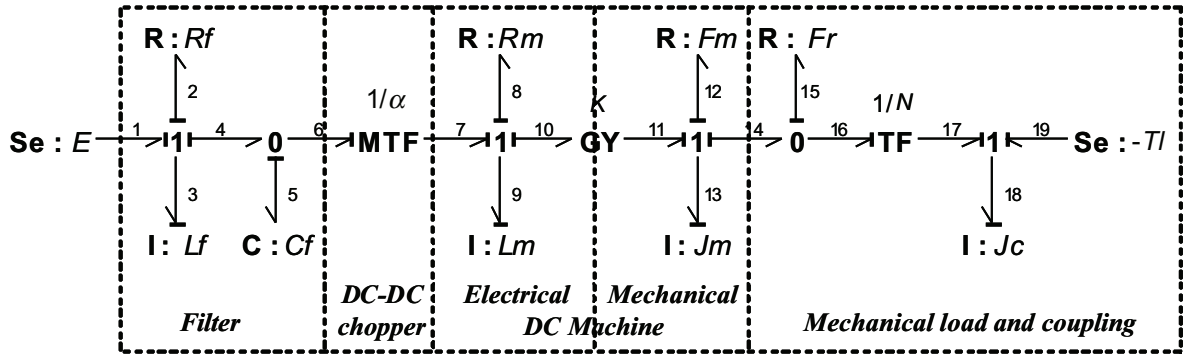

Fig. 5. Bond graph of the DC motor traction system.

II. BOND GRAPH BASED SYSTEM ANALYSIS METHODS

Several analysis can be directly applied on BGs :

- Firstly, structural analysis as model order, observability and commandability, can be deduced from BGs [3].
- Secondly, mathematical models such as transfer function and state equations can be directly derived from causal BGs [2]. The model modes can then be determined. By analysing these modes associated with the parameters values, stability analysis or coupling analysis can be characterised.
- Thirdly, several model simplification methods can be applied directly on BGs. One can speak about the Singular Perturbations Method (SPM) [6][9-10], which is based on the element dynamics, and the Model Order Reduction Algorithm (MORA) based on the energetic transfers [7-8][10-12].
- Finally, by using the concept of bicausality [13], the inverse BG model can be determined to synthesize the constraints with respect to requirements.

In our research, we have mainly considered the issue of model simplification [9-11] even if this paper is only focused on the stability analysis.

II.1. Bond Graph based Method for Local Stability Analysis

Analysing the system stability is of prime importance and the stability domain must be characterised to avoid risks of system damage. Being generally non linear, the system cannot be analysed on the whole range of parameters space. Thus, a linearised model around operating point has to be derived. In fact, all the variables of a non linear model can be written as :

$$\begin{aligned} X &= \overline{\mathbf{X}} + \Delta X \\ U &= \overline{\mathbf{U}} + \Delta U \end{aligned} \qquad \text{(eq. 3)}$$

where $\overline{\mathbf{X}}$ and $\overline{\mathbf{U}}$ represent respectively the values of state and input vectors at the operating point, while $\Delta\mathbf{X}$ and $\Delta\mathbf{U}$ are respectively their small variations.

Classically, the small signal model can be derived from the state equations. But this linearisation can also be directly applied on the BG by determining the linearised BG as presented in [12][14]. Several types of non linearities can exist :

- Non linear characteristics of passive (*R*, *C*, *I*) or active (*Se*, *Sf*) elements : for example, if an *R* dissipative element involves a non linear :

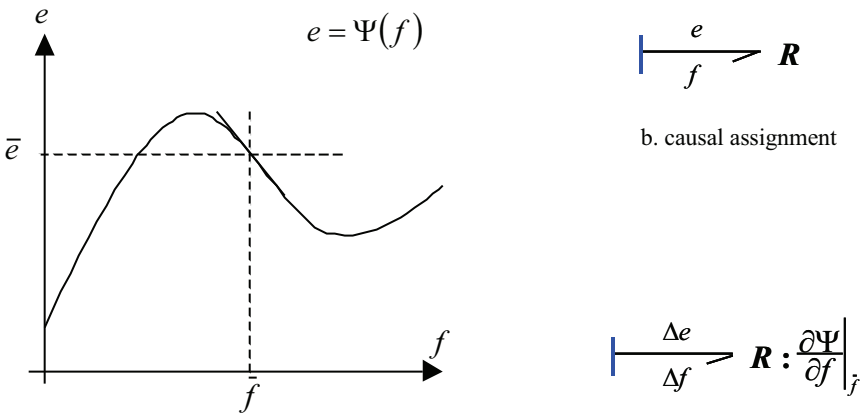

a. non linear characteristic

b. causal assignment

c. linearised element

Fig. 6. Linearisation of an *R* element.

- Non linear variation of an element modulus or of modulated gain for a *GY* (gyrator) or *TF* (transformer) junction :
  - Example of a non linear *I* element (integral causality) :

Non linear	Linearised
$\xrightarrow[f_1]{e_1} \boldsymbol{I}: \Psi(\beta)$	$\xrightarrow[\Delta f_1]{\Delta e_1} 0 \longrightarrow \boldsymbol{I}: \Psi(\bar{\beta})$ $\boldsymbol{MSf}: \bar{p}_1 . \Psi^{-2}(\bar{\beta}) \left.\frac{\partial \Psi}{\partial \beta}\right\|_{\bar{\beta}} \Delta\beta$
$f_1 := \Psi^{-1}(\beta) p_1$	$\Delta f_1 := \Psi^{-1}(\bar{\beta}) \Delta p_1 - \bar{p}_1 . \Psi^{-2}(\bar{\beta}) \left.\frac{\partial \Psi}{\partial \beta}\right\|_{\bar{\beta}} \Delta\beta$

  - Example of a modulated transformer :

Non linear	Linearised
$\xrightarrow[f_1]{e_1} \overset{m = \Psi(\beta)}{\boldsymbol{MTF}} \xrightarrow[f_2]{e_2}$	$\overset{\bar{m} = \Psi(\bar{\beta})}{\xrightarrow[\Delta f_1]{\Delta e_1} 1 \longrightarrow \boldsymbol{TF} \longrightarrow 0 \xrightarrow[\Delta f_2]{\Delta e_2}}$ $\boldsymbol{MSe}: -\bar{e}_2 . \left.\frac{\partial \Psi}{\partial \beta}\right\|_{\bar{\beta}} . \Delta\beta$ $\quad$ $\boldsymbol{MSf}: \bar{f}_1 . \left.\frac{\partial \Psi}{\partial \beta}\right\|_{\bar{\beta}} . \Delta\beta$
$e_1 := \Psi(\beta) e_2$ $f_2 := \Psi(\beta) f_1$	$\Delta e_1 := \Psi(\bar{\beta}) \Delta e_2 + \bar{e}_2 . \left.\frac{\partial \Psi}{\partial \beta}\right\|_{\bar{\beta}} . \Delta\beta$ $\Delta f_2 := \Psi(\bar{\beta}) \Delta f_1 + \bar{f}_1 . \left.\frac{\partial \Psi}{\partial \beta}\right\|_{\bar{\beta}} . \Delta\beta$

It can be observed that the linearised elements strongly depend on the causality assignment. Finally, the small signal model only includes small variations on control variables and on system inputs.

II.2. Example

To illustrate this method, we take the example of the DC traction system previously presented in Section 0. The following linearised BG is derived from the causal BG of Fig. 5.

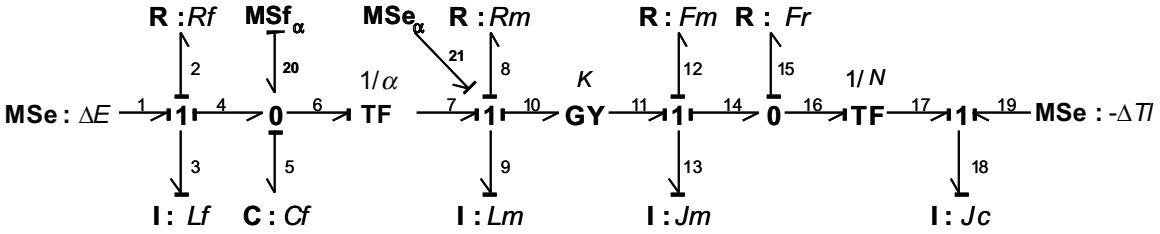

Fig. 7. Linearised BG of the DC traction system..

The small signal state equations can be deduced from this BG. The stability analysis of the open loop system can then be performed directly by analysing the root locus obtained from the linearised state equation.

In fact, several modulated inputs (MSf_α, MSe_α) are relative to the control variations of the DC-DC chopper ($\Delta\alpha$: duty cycle small variations) :

$$MSe_\alpha = \overline{e_6}.\Delta\alpha = \frac{\overline{q_5}}{C_f}.\Delta\alpha$$
$$MSf_\alpha = -\overline{f_7}.\Delta\alpha = -\frac{\overline{p_9}}{L_m}.\Delta\alpha \qquad \text{(eq. 4)}$$

The PI current controller can also be linearised to achieve the stability analysis of the closed loop system. From the controller equation :

$$\dot{\alpha} = \frac{1}{E}\left(K_P\left(\dot{I}_{ref} - \dot{I}_m\right) + K_I\left(I_{ref} - I_m\right)\right) \qquad \text{(eq. 5)}$$

The small signal variation of the duty cycle can be derived :

$$\Delta\dot{\alpha} = \frac{1}{ET_{CL}}\left(-\frac{\overline{\alpha}}{C_f}\Delta q_5 - \frac{\overline{q_5}}{C_f}\Delta\alpha + \frac{K}{J_m}\Delta p_{13}\right) \qquad \text{(eq. 6)}$$

by assuming that the current reference is kept constant ($\dot{I}_{ref} = \Delta I_{ref} = 0$) and that the controller parameters K_P and K_I are adjusted to compensate the motor electric pole :

$$K_P = \frac{L_m}{T_{CL}}$$
$$K_I = \frac{R_m}{T_{CL}} \qquad \text{(eq. 7)}$$

where T_{CL} represent the desired time constant in closed loop.

Finally, (eq. 8) gives the small signal state equation corresponding with the closed loop system :

$$\begin{bmatrix} \Delta\dot{p}_3 \\ \Delta\dot{p}_9 \\ \Delta\dot{p}_{13} \\ \Delta\dot{p}_{18} \\ \Delta\dot{q}_5 \end{bmatrix} = \begin{bmatrix} -\frac{R_f}{L_f} & 0 & 0 & 0 & -\frac{1}{C_f} \\ 0 & -\frac{R_m}{L_m} & -\frac{K}{J_m} & 0 & \frac{\bar{\alpha}}{C_f} \\ 0 & \frac{K}{L_m} & -\frac{F_m + F_r}{J_m} & \frac{N F_r}{J_c} & 0 \\ 0 & 0 & \frac{N F_r}{J_m} & -\frac{N^2 F_r}{J_c} & 0 \\ \frac{1}{L_f} & -\frac{\bar{\alpha}}{L_m} & 0 & 0 & 0 \end{bmatrix} \begin{bmatrix} \Delta p_3 \\ \Delta p_9 \\ \Delta p_{13} \\ \Delta p_{18} \\ \Delta q_5 \end{bmatrix} + \begin{bmatrix} 1 & \frac{0}{q_5} & 0 \\ 0 & \frac{q_5}{C_f} & 0 \\ 0 & 0 & 0 \\ 0 & \frac{0}{} & 1 \\ 0 & -\frac{p_9}{L_m} & 0 \end{bmatrix} \begin{bmatrix} \Delta E \\ \Delta\alpha \\ -\Delta C_{ch} \end{bmatrix} \quad \text{(eq. 8)}$$

where p_3, p_9, p_{13}, p_{18} and q_5 represent the generalised energy variables respectively associated with the L_f, L_m, J_m, J_l and C_f elements.

By using the numerical values, the root locus can be obtained, by considering a given operating point obtained with $I_{ref} = 100$ A and the motor angular speed $\Omega_m = 250$ Rd/s. For example, the influence of the filter inductance L_f on the pole locus is presented on Fig. 8. With the zoom, we see that for $L_f > 9$ mH, there are poles in the positive real plan. It indicates that the poles are unstable. As we can see in Fig. 9 this analysis is validated by temporal simulations which also validate the proposed approach.

Let notice that this analysis process can be rather complex to handle, especially as the controlled system becomes complex itself. However, some software tools like ARCHER [15] provide the state equations from the BG. Furthermore, symbolic calculation tools like Maple, Mathematica or Matlab are useful to derive the linearised state equations of the control unit. In this case study, the root locus has been obtained from Matlab.

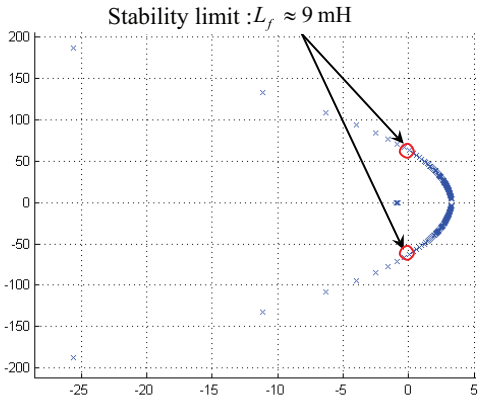

Fig. 8. Poles analysis : influence of the filter inductance value L_f.

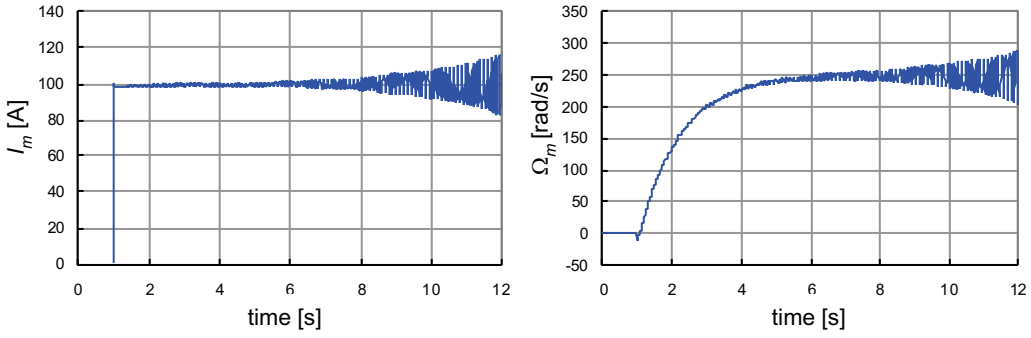

(a) $L_f = 10$ mH.

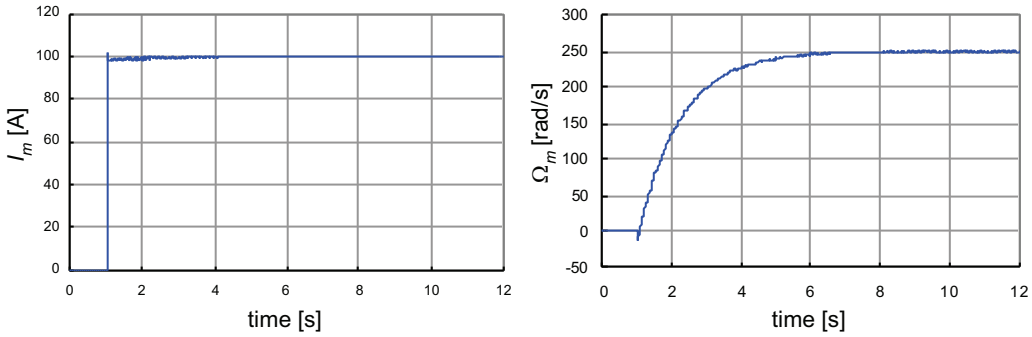

(b) L_f = 9 mH.

Fig. 9. Influence of the filter inductance value L_f on the motor current I_m and on the motor angular speed Ω_m : (a) unstable case (L_f = 10 mH) and (b) stable case (L_f = 9 mH)

III. Modelling of The Railway Traction System

A BB36000 railway traction system, produced by Alstom, France, is considered [12][16]. In fact, this case study is typical of the stability issues due to the existence of an input filter whose the natural frequency interacts both with the vector control bandwidth and with the resonant frequency of the mechanical transmission line. Simplifying the approach, only a single motor and transmission line is considered as presented on the synoptic of Fig. 19.

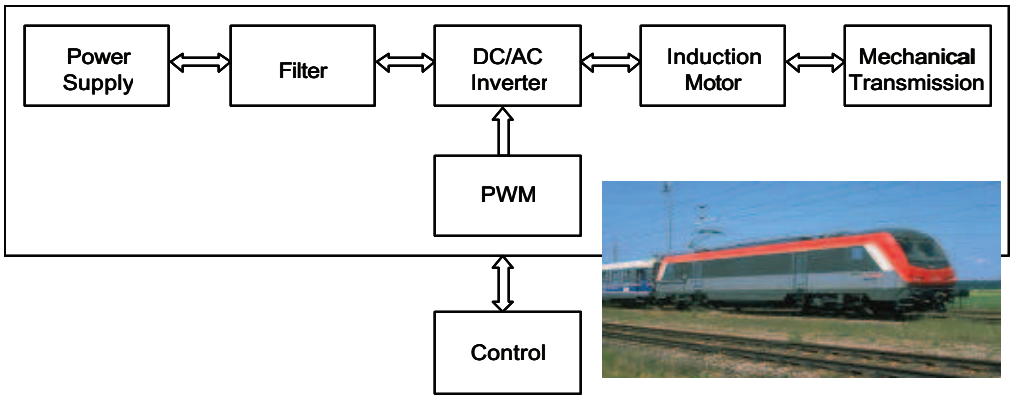

Fig. 10. The BB36000 simplified bloc diagram.

III.1. Power feeding

An ideal DC voltage source is considered and represented by an effort source **Se** : U_{cont}. This source feds an LCR filter to reduce the harmonic currents produced by the traction system and to filter perturbations caused by the power network (see Fig. 12).

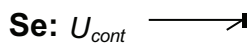

Fig. 11. Bond graph of alimentation source.

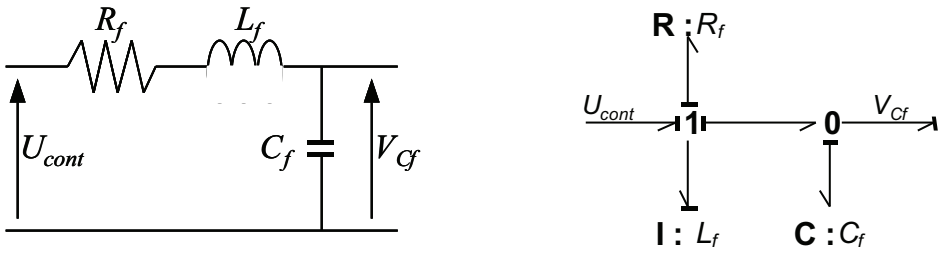

(a) (b)

Fig. 12. Input filter : (a) electrical circuit and (b) associated bond graph.

A three-phase alternating current is provided by a classical PWM voltage source inverter. In this model, each inverter leg is modelled by a modulated transformer whose gain is given by a control signal η_i (see Fig. 13). The PWM inverter can be modelled in average value (*MTF* modulated by the duty cycles) or in instantaneous value (*MTF* modulated by the conducting state of each leg).

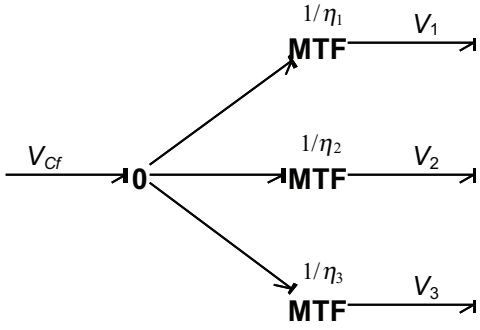

Fig. 13. BG model of the voltage source inverter.

III.2. Control unit

A classical Direct Field Oriented Control of the motor is used to independently regulate the rotor flux and the electromagnetic torque. Choosing PI controllers to obtain zero-error at steady state, this control unit is of order 2. The structure of the applied control is shown in Fig. 14. All variables are represented in a Park's reference frame (*d*,*q*) oriented along the rotor field.

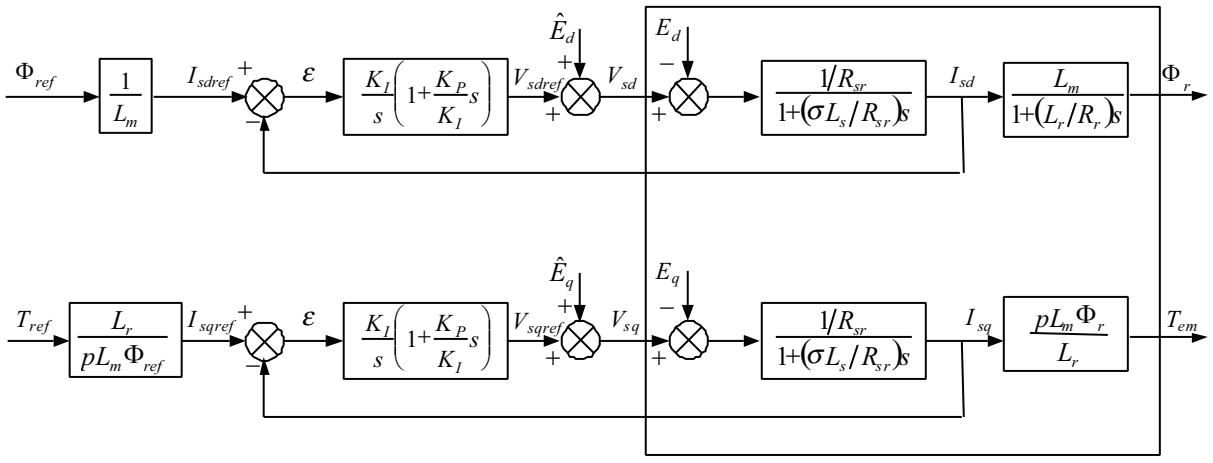

Fig. 14. Direct Field Oriented Control.

III.3. Induction motor

Squirrel cage induction motors drive the locomotive. Several BG models can be developed [9][12], following the considered equivalent circuit or following the chosen reference frame. Different reference frames are illustrated in Fig. 15, where indexes Φ and *V* are respectively used for the reference frame associated with the rotor flux and the stator voltage vector.

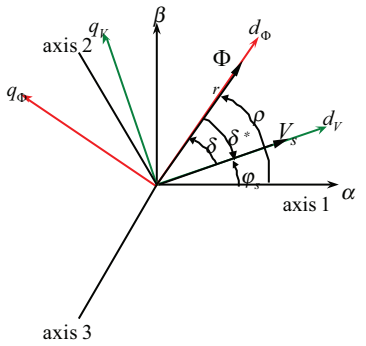

Fig. 15. Relations between reference frames.

Model A : Induction motor modelled in (α,β) fixed reference frame

To model the induction machine in a fixed reference frame, we have firstly chosen to totalise the leakage inductances on the stator side, (L_s, L_r, L_m) being respectively the stator, rotor and magnetising cyclic inductances and σ the leakage coefficient :

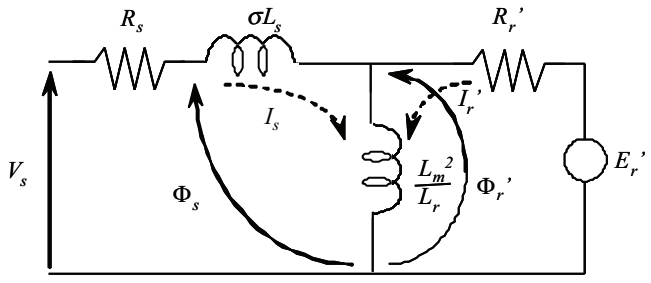

(a)

$$\sigma = 1 - \frac{L_m^{\,2}}{L_s L_r} \qquad R_r' = \left(\frac{L_m}{L_r}\right)^2 R_r$$

$$E'_{r\alpha,\beta} = \frac{L_m}{L_r} E_{r\alpha,\beta} \qquad I_r' = \frac{L_r}{L_m} I_r \qquad \Phi_r' = \frac{L_m}{L_r} \Phi_r$$

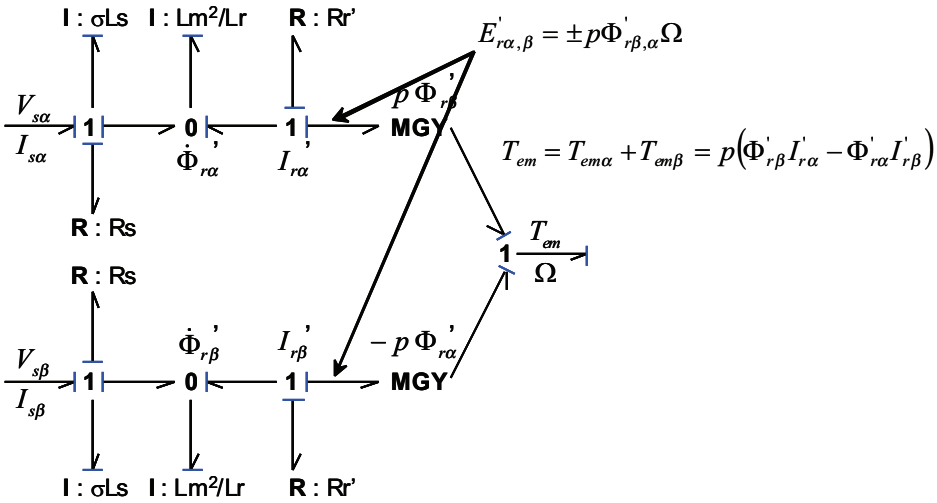

(b)

Fig. 16. induction motor model with totalised leakages inductances :
(a) equivalent circuit brought to the stator side and (b) associated bond graph.

Model B : Induction motor model in (d_V,q_V) reference frame linked to the stator voltage

The model previously presented was established in a fixed reference frame which involves alternating waves for electromagnetic variables. As the stability analysis issue is concerned, we have seen (cf. section III) that a small signal model must be set around a given operating point. Thus, when alternating variables are considered, as for an induction motor modelled in the (α,β) fixed reference

frame, the small signal linear model cannot be obtained because no operating point can be set, except of zero.

Therefore, an induction motor model established in a rotational reference frame must be considered. Classically, this can be made thanks to the Park's transformation. However, linearising the model including this latter transformation leads to linearise non linear cosine and sine terms which makes the approach more complex. In order to solve this issue, *an original model of the induction motor has been set by considering an orientation of the rotating reference frame (d_V,q_V) along the stator voltage vector :* $V_s = V_{sdV}$, $V_{sqV} = 0$.

This model depends on 2 inputs : the amplitude of stator voltage V_{sdV} and its pulsation ω_s. The first one can be determined from the inverter and its control. The last one can be calculated if we know the stator voltage phase φ_s. *Note that the derivation of the stator pulsation (ω_s) limits the utilisation of this model. Indeed, an instantaneous model of the inverter does not allow derivation of the phase angle which changes brutally. Thus, only an inverter modelled in average value can be associated with this particular model of the machine.*

The interest of this modelling is that the inverter can be represented by only one modulated transformer (see Fig. 17) whose the gain η_d is calculated as shown in Table 2. The input current of this converter is then the consequence of the power balance : $I_c = \eta_d . I_{sdV}$.

The associated bond graph of the induction machine modelled in this reference frame is displayed in Fig. 18.

Table 2. Stator voltage on the inverter output.

PWM inverter model	Stator voltage	
	Modelling in (α,β) reference frame	Modelling in (d,q) reference frame associated with the stator voltage vector
$V_1 = \left(\frac{2}{3}\alpha_1 - \frac{1}{3}\alpha_2 - \frac{1}{3}\alpha_3\right)V_{Cf}$ $V_1 = \left(\frac{2}{3}\alpha_1 - \frac{1}{3}\alpha_2 - \frac{1}{3}\alpha_3\right)V_{Cf}$ $V_1 = \left(\frac{2}{3}\alpha_3 - \frac{1}{3}\alpha_1 - \frac{1}{3}\alpha_2\right)V_{Cf}$	$V_{s\alpha} = \sqrt{\frac{2}{3}}.\left(V_1 - \frac{1}{2}V_2 - \frac{1}{2}V_3\right)$ $= \sqrt{\frac{2}{3}}.\left(\alpha_1 - \frac{1}{2}\alpha_2 - \frac{1}{2}\alpha_3\right)V_{Cf}$ $V_{s\beta} = \sqrt{\frac{1}{2}}.(V_2 - V_3) = \sqrt{\frac{1}{2}}.(\alpha_2 - \alpha_3)V_{Cf}$	$V_{sd} = \sqrt{{V_{s\alpha}}^2 + {V_{s\beta}}^2}$ $= \sqrt{\frac{1}{3}.\left(\begin{matrix}(\alpha_1-\alpha_2)^2 + (\alpha_1-\alpha_3)^2 \\ + (\alpha_2-\alpha_3)^2\end{matrix}\right)}.V_{Cf}$ $= \eta_d . V_{Cf}$

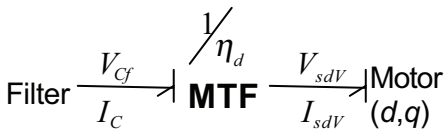

Fig. 17. Simple BG of the inverter for the induction motor modelled on the (d_V,q_V) reference frame.

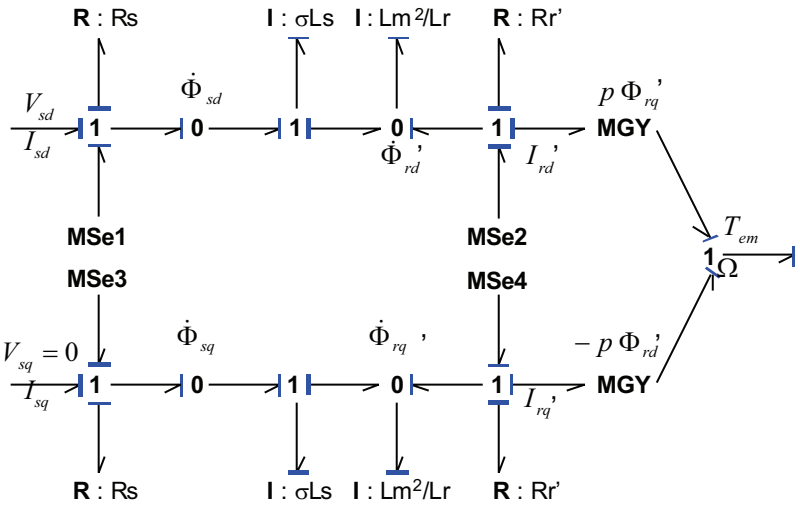

with

$$MSe_1 = \omega_s.\Phi_{sq}$$

$$MSe_2 = \omega_s.\Phi_{rq}'$$

$$MSe_3 = -\omega_s.\Phi_{sd}$$

$$MSe_4 = -\omega_s.\Phi_{rd}'$$

where

$$\Phi_r' = \frac{L_m}{L_r}\Phi_r$$

Fig. 18. Bond graph of induction motor modelled in the (d_V,q_V) reference frame.

III.4. Mechanical transmission line

The mechanical transmission line is constituted of 2 couplings. The motor inertia, followed by a first coupling on the primary shaft supplies a mobile reducer which is fixed on the locomotive body through a track link. At the reducer output, another coupling element, namely Jacquemin, is present before the wheel inertia. A complete description of the mechanical transmission line can be found in more details in [10][16]. A reduced BG model can be obtained for the low frequencies [9-10]. The synoptic of this line is presented in Fig. 19. The associated BG model is displayed in Fig. 20. In our modelling, we do not consider the wheel-rail contact which is modelled without sliding. With this hypothesis, the model is of 11th order.

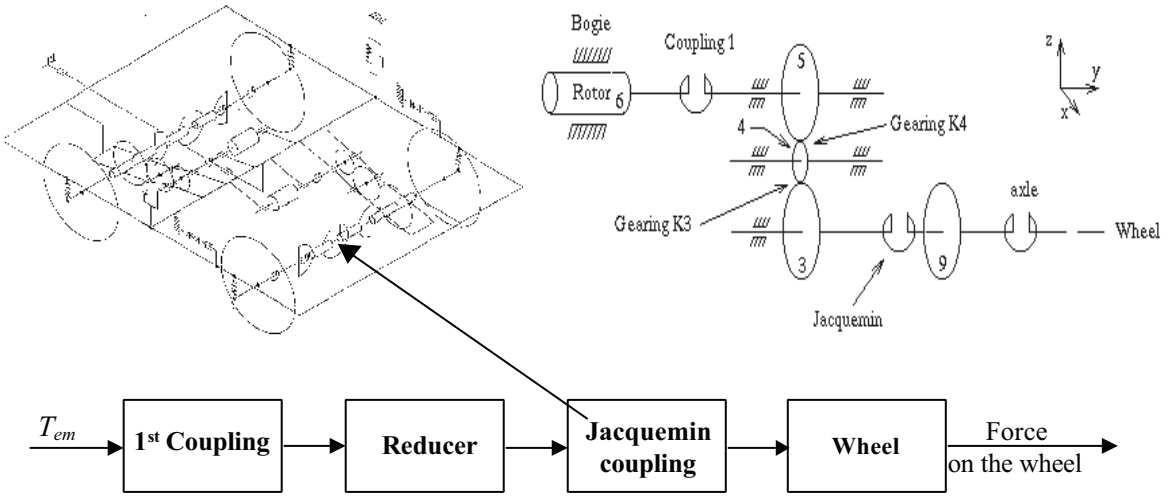

Fig. 19. Synoptic of the mechanical transmission line.

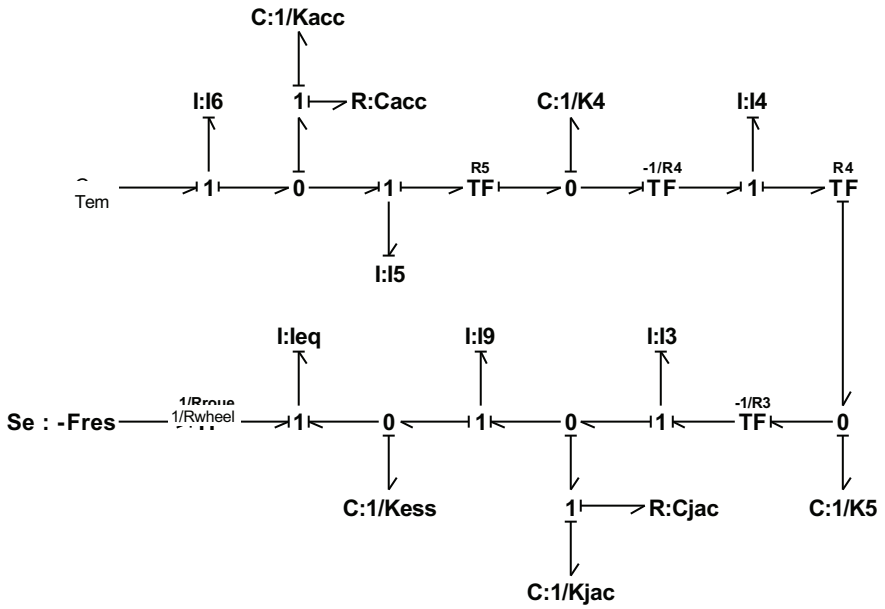

Fig. 20. Associated bond graph of the mechanical transmission line.

III.5. Validations by simulations

We validate our models by simulations. In particular, the two models of the induction machine are compared :

- Model A is the one with an induction motor modelled in the (α,β) fixed reference frame with leakage totalised on the stator side,
- Model B, is the one modelled in the rotating reference frame linked to the voltage (d_V,q_V).

For all models, 2 different cases are examined :

- a normal operating mode (system starting),
- a degraded operating mode obtained by short-circuiting one leg of the inverter.

Every model is simulated with the PWM inverter modelled in average value because the second model (B) is not valid for instantaneous operations. Fig. 21 and Fig. 22 show that all models have similar responses in a normal and a degraded operating mode which validates the original approach proposed for Model B.

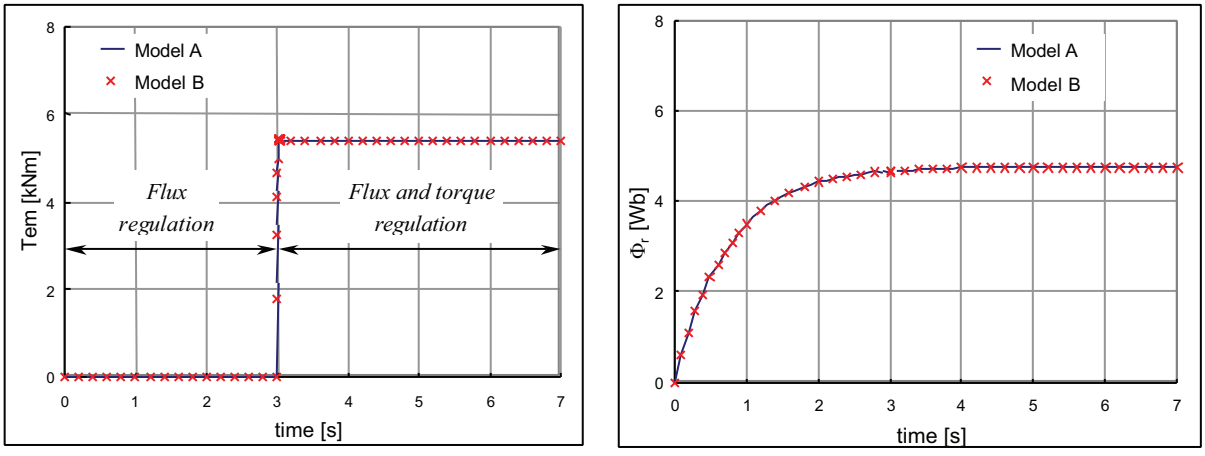

Fig. 21. A starting transient mode.

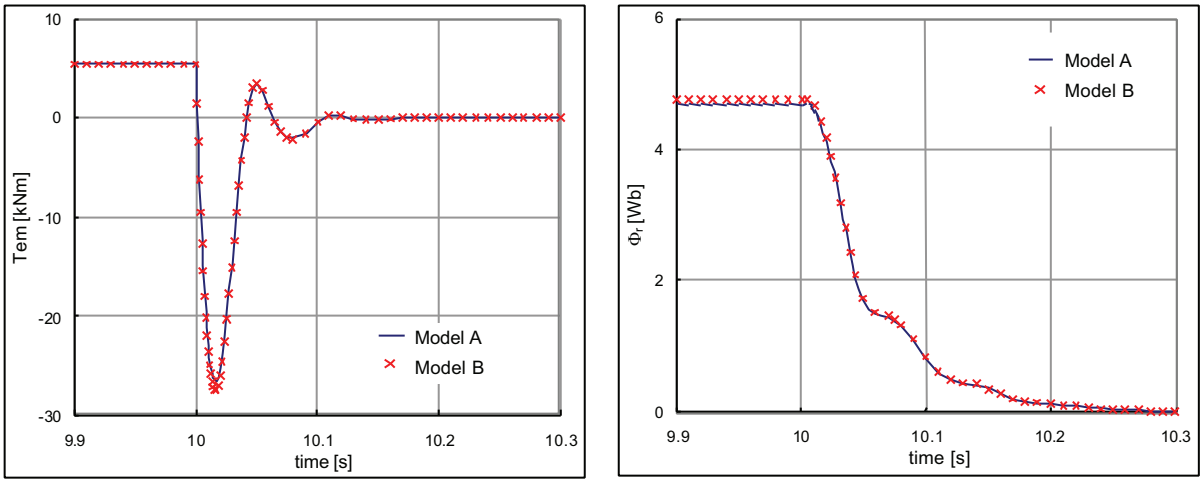

(a) (b)

Fig. 22. A short-circuit of one inverter leg.

IV. STABILITY ANALYSIS OF THE RAILWAY TRACTION MODELS

IV.1. BG based stability analysis procedure

We apply the stability analysis procedure previously presented in Section II. We have explained in Section III.3 that the models of the induction motor in the (α,β) reference frame can not be linearised. Therefore, we consider the induction motor modelled in the (d_V,q_V) reference frame linked to the voltage vector for the stability analysis of the railway traction system. To simplify the analysis, the mechanical part is here represented only by an inertia J_m (equivalent to the I_6), a friction f and a load torque T_l.

- **1st step : Small signal BG derivation**

As for the example of the DC traction system (see section II) the linearised BG of the railway traction system can be directly derived from the causal BG (see Fig. 23).

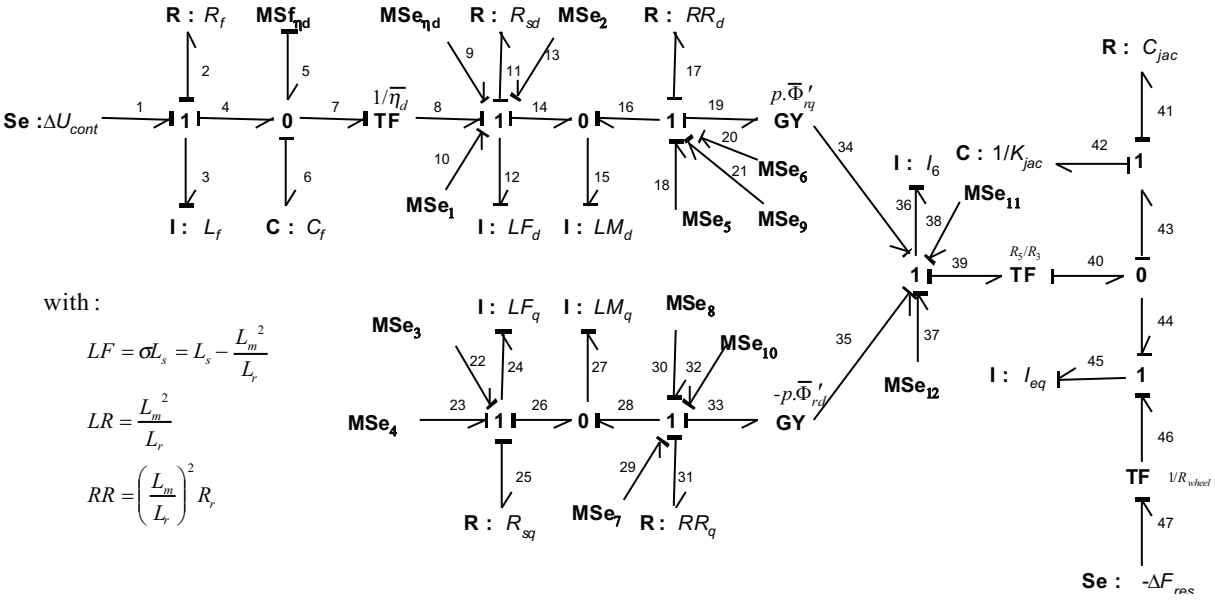

Fig. 23. Linearised BG of the railway traction system

On this BG, the elements *MSe* and *MSf* are associated with :

$\boxed{MSf_{\eta d} = -\bar{I}_{sd}.\Delta\eta_d}$ $\boxed{MSe_4 = -\overline{\Phi}_{sd}.\Delta\omega_s}$ $MSe_9 = -p.\overline{\Omega}.\Delta\Phi_{rq}'$ Control inputs

$\boxed{MSe_{\eta d} = \overline{V}_{Cf}.\Delta\eta_d}$ $MSe_5 = \overline{\omega}_s.\Delta\Phi_{rq}'$ $MSe_{10} = p.\overline{\Omega}.\Delta\Phi_{rd}'$

$MSe_1 = \overline{\omega}_s.\Delta\Phi_{sq}$ $\boxed{MSe_6 = \overline{\Phi}_{rq}'.\Delta\omega_s}$ $MSe_{11} = p.\bar{I}_{rd}.\Delta\Phi_{rq}'$

$\boxed{MSe_2 = \overline{\Phi}_{sq}.\Delta\omega_s}$ $MSe_7 = -\overline{\omega}_s.\Delta\Phi_{rd}'$ $MSe_{12} = -p.\bar{I}_{rq}.\Delta\Phi_{rd}'$

$MSe_3 = -\overline{\omega}_s.\Delta\Phi_{sd}$ $\boxed{MSe_8 = -\overline{\Phi}_{rd}'.\Delta\omega_s}$

The inputs of this linearised (small signal) BG are relative to the control unit (i.e. $\Delta\eta_d$, $\Delta\omega_s$).

- **2nd step : Stability analysis of the open loop system**

The stability of the open loop system can be analysed from that small signal BG by deducing the state equations. This can be made by means of the ARCHER software. When a simplified mechanical system is considered only including an inertia, a viscous friction and a load torque, the open loop system is of order 7. The state vector is then composed of :

$$\Delta\mathbf{X} = \left[\Delta I_{Lf} \quad \Delta V_{Cf} \quad \Delta I_{sdV} \quad \Delta I_{sqV} \quad \Delta\Phi_{rdV} \quad \Delta\Phi_{rqV} \quad \Delta\Omega\right]^T \qquad \text{(eq. 9)}$$

Finally, the analysis of the root locus allows to determine the stability domain.

- **3rd step : Stability analysis of the closed loop system**

However, for such systems, the control bandwidth strongly influences the stability. Thus, closed loop operation must be considered by including the control unit in the analysis as presented in the example of the DC traction system (see section III).

For that purpose, the control outputs ($\Delta\eta_d$, $\Delta\omega_s$) have to be calculated from the control equations.

- ***Calculation of*** $\Delta\eta_d$ ***:***

$$\Delta\eta_d = \Delta\left(\frac{V_{sdV}}{V_{Cf}}\right) = \frac{\Delta V_{sdV}}{\overline{V_{Cf}}} - \frac{\overline{V_{sdV}}.\Delta V_{Cf}}{\overline{V_{Cf}}^2} \qquad \text{(eq. 10)}$$

The motor input voltage is defined as :

$$V_{sdV} = \sqrt{V_{sdref\Phi}^2 + V_{sqref\Phi}^2} \qquad \text{(eq. 11)}$$

The linearisation of this voltage then leads to :

$$\Delta V_{sdV} = \frac{1}{V_{sdV}}\left(\overline{V_{sdref\Phi}}.\Delta V_{sdref\Phi} + \overline{V_{sqref\Phi}}.\Delta V_{sqref\Phi}\right) \qquad \text{(eq. 12)}$$

Thus, the small signal state equations can be established as (eq. 13). The inputs of this latter model are (ΔU_{cont}, $\Delta V_{sdref\Phi}$, $\Delta V_{sqref\Phi}$, $\Delta\omega_s$). The control inputs ($\Delta V_{sdref\Phi}$, $\Delta V_{sqref\Phi}$, $\Delta\omega_s$) can also be developed. In our case study, the field oriented control strategy involves control variables operating in another (d_Φ,q_Φ) reference frame linked to the rotor field. A classical strategy of rotor flux oriented control presented on Fig. 14 is considered. However, in order to simplify the complex development leading to the linearised control, we have neglected the electromotive forces (E_d and E_q) which decouple the current controllers (see Fig. 14). Then, the control state equations can be expressed as (eq. 14), where T_{ref} and Φ_{ref} represent the reference values of the electromagnetic torque and the rotor flux, and the Φ_r term is defined as $\Phi_r = \sqrt{\Phi_{rdV}^2 + \Phi_{rqV}^2}$.

$$\frac{d}{dt}\Delta I_{Lf} = \frac{1}{L_f}\left(-R_f.\Delta I_{Lf} - \Delta V_{Cf} + \Delta U_{cont}\right)$$

$$\frac{d}{dt}\Delta V_{Cf} = \frac{1}{C_f}\begin{pmatrix} \Delta I_{Lf} - \dfrac{\overline{V_{sdV}}}{\overline{\overline{V_{Cf}}}}\Delta I_{sdV} + \dfrac{\overline{V_{sdV}}.\overline{I_{sdV}}}{\overline{V_{Cf}}^{2}}\Delta V_{Cf} \\ -\dfrac{\overline{I_{sdV}}}{\overline{\overline{V_{Cf}}}.\overline{V_{sdV}}}\left(\overline{V_{sdref\Phi}}.\Delta V_{sdref\Phi} + \overline{V_{sqref\Phi}}.\Delta V_{sqref\Phi}\right) \end{pmatrix}$$

$$\frac{d}{dt}\Delta I_{sdV} = \frac{1}{\sigma L_s}\begin{pmatrix} \dfrac{1}{\overline{\overline{V_{sdV}}}}\left(\overline{V_{sdref\Phi}}.\Delta V_{sdref\Phi} + \overline{V_{sqref\Phi}}.\Delta V_{sqref\Phi}\right) - R_{sr}.\Delta I_{sdV} + \dfrac{L_m}{L_r^{2}}R_r.\Delta\Phi_{rdV} \\ +\sigma L_s.\overline{I_{sqV}}.\Delta\omega_s + \sigma L_s.\Delta I_{sqV}.\overline{\omega_s} + p\dfrac{L_m}{L_r}.\overline{\Phi_{rqV}}.\Delta\Omega + p\dfrac{L_m}{L_r}.\Delta\Phi_{rqV}.\overline{\Omega} \end{pmatrix}$$

(eq. 13)

$$\frac{d}{dt}\Delta I_{sqV} = \frac{1}{\sigma L_s}\begin{pmatrix} -R_{sr}.\Delta I_{sqV} + \dfrac{L_m}{L_r^{2}}R_r.\Delta\Phi_{rqV} - \sigma L_s.\overline{I_{sdV}}.\Delta\omega_s - \sigma L_s.\Delta I_{sdV}.\overline{\omega_s} \\ -p\dfrac{L_m}{L_r}.\overline{\Phi_{rdV}}.\Delta\Omega - p\dfrac{L_m}{L_r}.\Delta\Phi_{rdV}.\overline{\Omega} \end{pmatrix}$$

$$\frac{d}{dt}\Delta\Phi_{rdV} = \frac{R_r}{L_r}\left(L_m.\Delta I_{sdV} - \Delta\Phi_{rdV}\right) + \overline{\Phi_{rqV}}\left(\Delta\omega_s - p.\Delta\Omega\right) + \Delta\Phi_{rqV}\left(\overline{\omega_s} - p.\overline{\Omega}\right)$$

$$\frac{d}{dt}\Delta\Phi_{rqV} = \frac{R_r}{L_r}\left(L_m.\Delta I_{sqV} - \Delta\Phi_{rqV}\right) - \overline{\Phi_{rdV}}\left(\Delta\omega_s - p.\Delta\Omega\right) - \Delta\Phi_{rdV}\left(\overline{\omega_s} - p.\overline{\Omega}\right)$$

$$\frac{d}{dt}\Delta\Omega = \frac{1}{J_m}\left(p\frac{L_m}{L_r}\left(\overline{\Phi_{rdV}}.\Delta I_{sqV} + \Delta\Phi_{rdV}.\overline{I_{sqV}} - \overline{\Phi_{rqV}}.\Delta I_{sdV} - \Delta\Phi_{rqV}.\overline{I_{sdV}}\right) - f.\Delta\Omega - \Delta T_l\right)$$

$$\begin{aligned} \frac{d}{dt}V_{sdref\Phi} &= K_I\left(\frac{\Phi_{ref}}{L_m} - I_{sd\Phi}\right) + K_p\frac{d}{dt}\left(\frac{\Phi_{ref}}{L_m} - I_{sd\Phi}\right) \\ &= K_I\left(\frac{\Phi_{ref}}{L_m} - I_{sd\Phi}\right) - K_p\frac{d}{dt}\left(I_{sd\Phi}\right) \\ \frac{d}{dt}V_{sqref\Phi} &= K_I\left(\frac{L_rT_{ref}}{pL_m\Phi_r} - I_{sq\Phi}\right) + K_p\frac{d}{dt}\left(\frac{L_rT_{ref}}{pL_m\Phi_r} - I_{sq\Phi}\right) \\ &= K_I\left(\frac{L_rT_{ref}}{pL_m\Phi_r} - I_{sq\Phi}\right) - K_p\left(\frac{L_rT_{ref}}{pL_m\Phi_r^{2}}\frac{d}{dt}\left(\Phi_r\right) + \frac{d}{dt}\left(I_{sq\Phi}\right)\right) \end{aligned}$$

(eq. 14)

- ***Calculation of*** $\Delta\omega_s$ ***:***

The pulsation ω_s is the angular velocity of the angle φ_s, where $\varphi_S = \rho + \delta^*$. Then,

$$\omega_s = \frac{d}{dt}\varphi_s = \frac{d}{dt}\rho + \frac{d}{dt}\delta^* = \omega_\rho + \omega_{\delta^\mu} \qquad \text{(eq. 15)}$$

By using autopiloting equation, the pulsation ω_ρ can be formulated as :

$$\omega_\rho = \omega + \frac{R_r L_m I_{sq\Phi}}{L_r \Phi_r} \qquad \text{(eq. 16)}$$

The angle δ^* can be calculated from (eq. 17).

$$\delta^* = \arctan\left(\frac{V_{sqref\Phi}}{V_{sdref\Phi}}\right) \qquad \text{(eq. 17)}$$

Its derivation, the ω_{δ^*} term, can be defined as :

$$\omega_{\delta^*} = \frac{V_{sdref\Phi}\frac{d}{dt}\left(V_{sqref\Phi}\right) - V_{sqref\Phi}\frac{d}{dt}\left(V_{sdref\Phi}\right)}{V_{sdref\Phi}^{\ 2} + V_{sqref\Phi}^{\ 2}} \qquad \text{(eq. 18)}$$

By using (eq. 15), (eq. 16) and (eq. 18), we obtain the angular velocity ω_s. The variation of this pulsation can then be deduced.

The complex linearisation of these expressions is detailed in [12]. It allows to enhance the order of the state equation (9th order) as :

$$\Delta\mathbf{X} = \left[\Delta I_{Lf} \quad \Delta V_{Cf} \quad \Delta I_{sdV} \quad \Delta I_{sqV} \quad \Delta\Phi_{rdV} \quad \Delta\Phi_{rqV} \quad \Delta\Omega \quad \Delta V_{sdref\Phi} \quad \Delta V_{sqref\Phi}\right]^T \qquad \text{(eq. 19)}$$

This small signal model depends on the physical system parameters but also on the control requirement through the controller parameters (K_P and K_I).

By means of the Matlab© software, the stability domain can be characterised by analyzing the root locus of the closed loop system linearised around an operating point defined by the reference parameters (T_{ref}, Φ_{ref}) and of the load (T_l).

In the following simulations, the rated operating point is defined by : T_{ref} = 5 kNm, Φ_{ref} =6 Wb et T_l = 4998 Nm, which sets the motor angular speed at 20 rad/s.

IV.2. Analysis results of the railway traction system stability

- **Influence of the filter capacitor value C_f**

We have firstly investigated the stability of the operating point as a function of the filter capacitor value C_f which varies here between 1 and 100 mF. Fig. 24 presents the poles locus. The arrows show the poles propagation direction when the C_f value increases. For this particular operating point (T_{ref} = 5 kNm, Ω = 20 Rd/s, *Power* = 100 kW), it can be seen that the model is unstable for C_f < 1.3 mF.

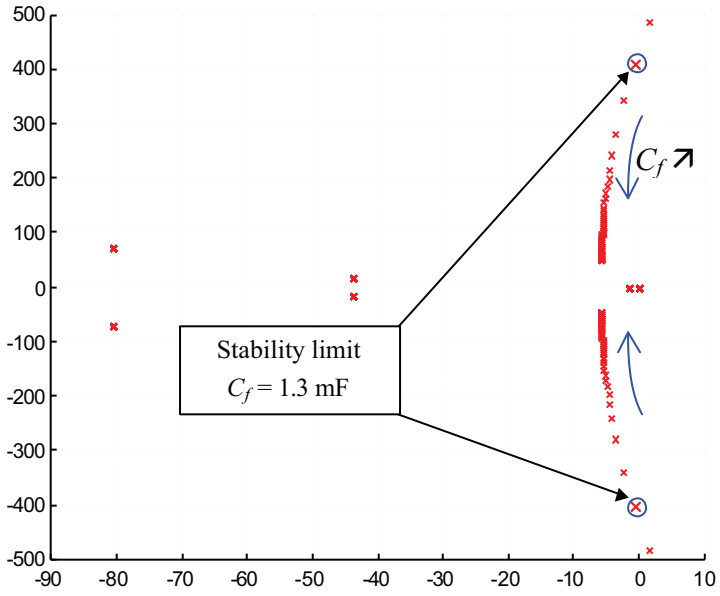

Fig. 24. Influence of the filter capacitor value C_f.

- **Influence of the control bandwidth**

We examine the influence of this parameter value by setting the closed loop time constant from T_{CL} = 1 ms to T_{CL} = 100 ms. In this range, and for the rated filter capacitor of 17mF, we do not find unstable zones. However, reducing this latter parameters or varying the rotation speed could lead to unstability.

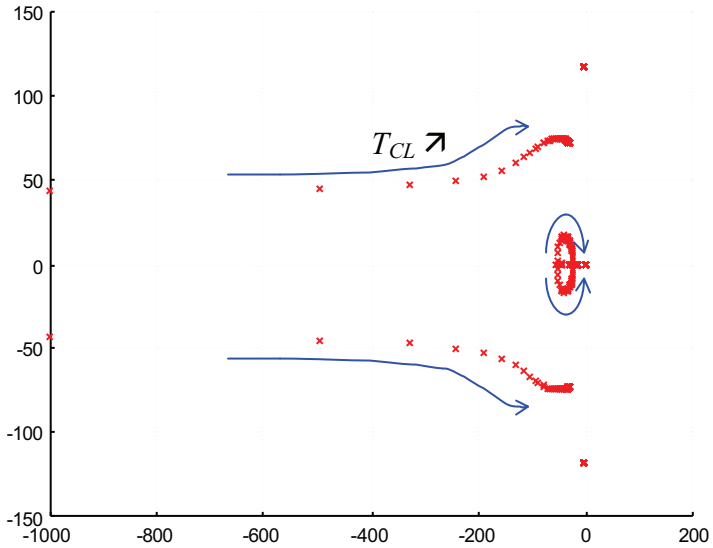

Fig. 25. Influence of the controller time constant value T_{CL}.

- **Influence of the mechanical angular speed Ω**

The investigated range of this latter parameter is between 0 and 100 Rd/s. For a rated value of the filter capacitor (C_f = 17 mF), the model is always stable. However, when we use a reduced value of filter capacitor (C_f = 3 mF), there is an unstable doma in when Ω ≥ 51 Rd/s.

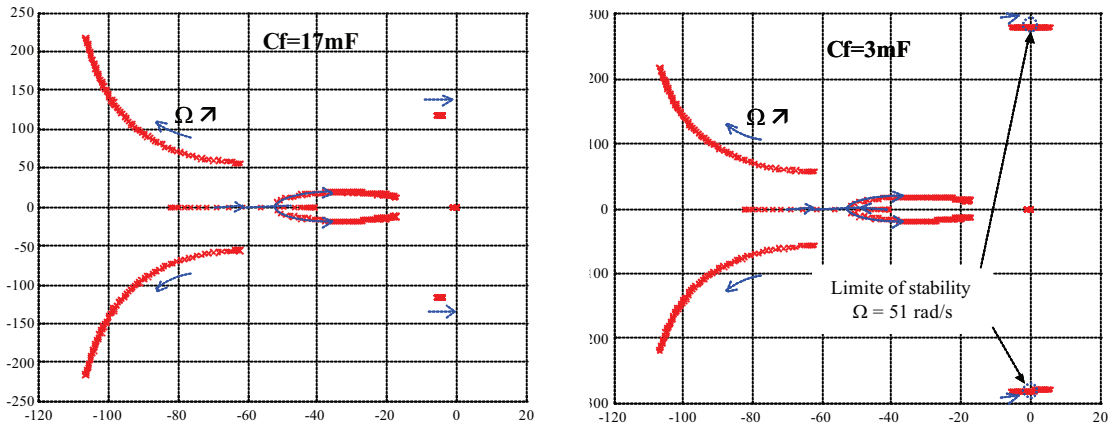

Fig. 26. Influence of the motor mechanical angular speed Ω.

IV.3. Validation of the analysis procedure

In this section, we verify the stability analysis procedure by simulating the non linear BG model of the traction system. A reduced value of the filter capacitor (C_f = 3 mF) is set. Four different states are simulated (see Fig. 27) :

- *State 1* : the angular speed is null (a null load torque is applied).
- *State 2* : the angular speed increases with an important gradient (first transient state) because we use only one tenth of the train mass to accelerate the simulation.
- *State 3* : it is the second transient state where we use the whole train inertia.
- *State 4* : the desired load is applied to set the operating point at steady state of the speed.

We present in Fig. 27 the simulation results for the motor mechanical angular speed Ω = 60 Rd/s. These figures show the instability where oscillation variables are amplified.

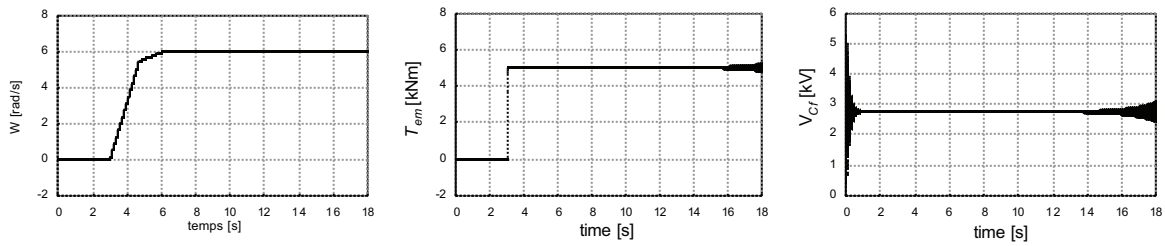

Fig. 27. Influence of the motor mechanical angular speed Ω : unstable operating points.

For the mechanical speed of Ω = 55 Rd/s, it can be seen from the zoom on the capacitor voltage that an unstable behaviour is obtained. The system is stable for Ω = 50 Rd/s.

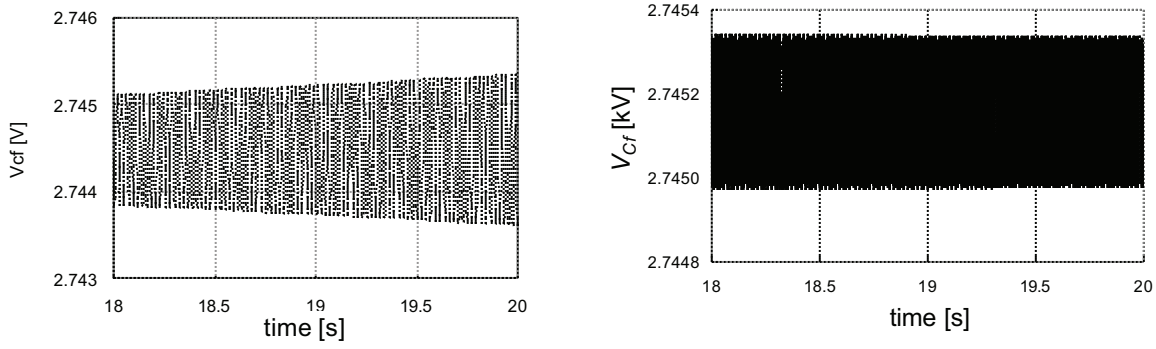

(a) (b)

Fig. 28. Tests for : (a) $\Omega^{(static)}$ = 55 Rd/s and (b) $\Omega^{(static)}$ = 50 Rd/s.

Note that equivalent results have been obtained thanks to the previous stability analysis procedure based on the BG approach, which proves its validity.

For $C_f = 17\,\text{mF}$, we have verified by simulations that the system is always stable as indicated in the analysis procedure.

V. CONCLUSIONS

In this paper, a homogeneous BG model of a railway traction system has been presented allowing to emphasise the electromechanical couplings. We have mainly focused our attention on a stability analysis procedure that can be directly deduced from the BG model. For that purpose, the BG has to be linearised around an operating point. We have also proposed an original model of the induction motor, represented in the (d_V,q_V) rotating reference frame related to the stator voltage vector. This model allows to avoid the non linear Park's transformation which makes easier to linearise the BG and to obtain a small signal model. The influence of system parameters on the stability has then be investigated and validated by simulations on the non linear model.

This work is a contribution showing how the Bond Graph formalism is useful for modelling and analysing electrical engineering multi-field systems. Indeed, obtaining a homogeneous modelling greatly facilitates the system approach by emphasising couplings in spite of physical fields crossing. More particularly, we have shown in this contribution, how this methodology is convenient for the local stability analysis. Of course, the same kind of analysis could be done from the state model through its linearisation around the same operating point. The Bond Graph formalism can then be seen as a powerful alternative allowing a systematic and structured approach from which the linearised model of an energetic system can be systematically deduced. As the stability analysis of a closed loop controlled system is concerned, a signal part (control part) is associated with the causal Bond Graph (energetic part). The linearisation of the signal part can only be done by means of state equations derivation of the control strategy, which greatly contributes to the complexity of the analysis as it was emphasised on the typical example of a railway traction system.

More generally, this contribution on system stability is a complement of other studies dedicated to model reduction and other issues particularly useful for system design.

REFERENCES

[1]. H. Paynter, *Analysis and Design of engineering systems*, MIT Press, 1961.

[2]. D. Karnopp, D. Margolis, R. Rosenberg, *System Dynamics : Modelling and Simulation of Mechatronic Systems*, John Wiley & sons, 2000 (3rd edition).

[3]. G. Dauphin-Tanguy, *Les Bond Graphs*, édition Hermès, Paris, 2000.

[4]. C. Sueur and G. Dauphin-Tanguy, "Bond-graph approach for structural analysis of MIMO linear systems," *Journal of the Franklin Institute* vol. 328, pp. 55-70, Pergamon Press, 1991.

[5]. G. Dauphin-Tanguy, A. Rahmani, C. Sueur, "Bond graph aided design of controlled systems," *Simulation Practice and Theory*, No. 7, pp. 493-513, Elsevier Science B.V., 1999.

[6]. C. Sueur, G. Dauphin Tanguy, "Bond Graph Approach to Multi-time Scale Systems Analysis," *Journal of the Franklin Institute* vol. 328, pp. 1005-1026, Pergamon Press, 1991.

[7]. L.S Louca, J.L. Stein, G.M. Hulbert, "A Physical-based Model reduction Metric with an Application to Vehicle Dynamics," *Proceedings of 4th IFAC Nonlinear Control Systems Symposium*, Enschede, The Netherlands, 1998.

[8]. L.S. Louca, J.L. Stein, "Energy-based Model Reduction of Linear Systems," *Proceedings of International Conference on Bond Graph Modelling and Simulation ICBGM'99*, volume 31, San Francisco, CA, 1999.

[9]. G. Gandanegara, B. Sareni, X. Roboam, G. Dauphin-Tanguy, Bond Graph Multi-time Scale Analysis of a Railway Traction System, EPE'01 conference, Graz, Austria, September 2001.

[10]. G. Gandanegara, X. Roboam, B. Sareni, G. Dauphin-Tanguy, "Modeling and Multi-time Scale Analysis of Railway Traction Systems Using Bond Graphs," *Proceedings of International Conference on Bond Graph Modeling and Simulation ICBGM'01*, Phoenix, 2001.

[11]. G. Gandanegara, X. Roboam, B. Sareni and G. Dauphin-Tanguy, "One Model for One Frequency Range : Comparison of Bond Graph Based Simplification Methods," *Proceedings of International Conference on Bond Graph Modeling and Simulation ICBGM'03*, Orlando, 2003.
[12]. G. Gandanegara, *Methodologie de conception systémique en genie Electrique à l'aide de l'outil Bond Graph : Application à une chaîne de traction ferroviaire*, Thesis INP Toulouse, November 2003.
[13]. P.J. Gawthrop, "Bicausal Bond Graph," *Proceedings of International Conference on Bond Graph Modeling and Simulation ICBGM'95*, volume 27, pp 83-88, 1995.
[14]. D. Karnopp, "Power and Energy in Linearised Physical Systems," *Journal of the Franklin Institute*, Vol. 303, No. 1, pp. 86-98, Pergamon Press, January 1977.
[15]. A. Azmani and G. Dauphin-Tanguy, "ARCHER: a program for computer aided modelling and analysis," *Bond graph for Engineers*. Ed. G. Dauphin-Tanguy and P. Breedveld, Elsevier Science Pub., pp. 263-278, 1992.
[16]. C. Lochot, X. Roboam, B. de Fornel, F. Moll, "High speed railway traction system modelling for simulating electromechanical interactions," *World Conference on Railway Research (WCRR'97)*, November 1997, Firenze, Italy.

THE AUTHORS

Grace Gandanegara received her Ph.D. degree in Control Systems from the Institut National Polytechnique of Toulouse, France, in 2003. She is currently post doctoral researcher at the Laboratory of Electrotechnics and Industrial Electronics (LEEI) of Toulouse. Her research interests include the analysis and system design in electrical engineering with bond graph methods.

Xavier ROBOAM received the PHD Degree in Electrical Engineering from the Institut National Polytechnique of Toulouse, FRANCE in 1991. He has been in the Laboratory of Electrotechnics and Industrial Electronics (LEEI) of Toulouse since 1992 as a full-time researcher. Since 1998, he is head of the team ''SYSTEM'' whose the objective is to process the design problem at a "system level". He develops methodologies specifically oriented towards multi-fields systems design for applications such as electrical embedded systems or renewable energy systems.

Bruno Sareni is assistant professor in Electrical Engineering and Control Systems Department at the Institut National Polytechnique of Toulouse, France. He is also researcher at the Laboratory of Electrotechnics and Industrial Electronics (LEEI) of Toulouse. He received his Ph.D. degree in 1999 from the Ecole Centrale de Lyon. His research activities are related to the analysis of complex heterogeneous power devices in electrical engineering with bond graph methods and the optimization of these systems using artificial evolution algorithms.

Genevieve Dauphin-Tanguy (senior member IEEE), graduated from University of Lille, France (BSc Physics, BSc Mathematics, MSc Mechanics) and from the french Grande Ecole d'Ingénieurs, Ecole Centrale de Lille (State Engineering Diploma), received the Ph.D. in 1981 and the Doctorate of Sciences in 1983 both from University of Lille. She is presently Professor of Control Design at Ecole Centrale de Lille and Head of the research group "Bond graph models" in the Laboratoire d'Automatique Génie Informatique et Signal (LAGIS associated with the CNRS, french National Center For Scientific Research). She is expert for the French Ministry of Education and Research. She is mainly engaged in the research fields of Modelling, Analysis, Control and Monitoring of systems by using the bond-graph tool. Her application domains are mechatronics in car industry and aeronautics and thermofluid processes (fuel cells).